STATE RESEARCH CENTER OF RUSSIA

INSTITUTE FOR HIGH ENERGY PHYSICS

IHEP 99–37

A.V. Sannikov, E.N. Savitskaya

PHYSICS OF THE HADRON CODE: RECENT STATUS AND COMPARISON WITH EXPERIMENT

Submitted to *NIM*

Protvino 1999

UDK 539.1.01 M–24

Abstract

Sannikov A.V., Savitskaya E.N. Physics of the HADRON Code: Recent Status and Comparison with Experiment: IHEP Preprint 99–37. – Protvino, 1999. – p. 12, figs. 12, refs.: 34.

A recent version of the high energy transport code HADRON is described in part of the hadron event generator. The improved cascade-exciton model was extensively tested by the experimental data for double differential cross sections for the (N, xN')-reactions. Good agreement with experiment in wide ranges of nucleon energies and target nuclei confirms reliability of the new physical model. The ways of further improvement are under discussion.

Аннотация

Санников А.В., Савицкая Е.Н. Физика программы HADRON: современное состояние и сравнение с экспериментом: Препринт ИФВЭ 99–37. – Протвино, 1999. – 12 с., 12 рис., библиогр.: 34.

Описана современная версия программы переноса высокоэнергетических адронов HADRON в части адронного генератора. Проведено подробное сравнение модифицированной каскадно-экситонной модели с экспериментальными данными по двойным дифференциальным сечениям для $(N,\ xN')$-реакций. Хорошее согласие с экспериментом в широком диапазоне энергий нуклонов и ядер-мишеней подтверждает достоверность новой физической модели. Обсуждаются пути дальнейшего усовершенствования программы.

1. Introduction

Many models of non-equilibrium nuclear reactions were developed in the last decades. The first one and most popular of them is the cascade model [1] describing nuclear reaction in a semiclassical way as a series of hadron-nucleon collisions in a nuclear potential well. Another semiclassical theory is the exciton model realizing in its different modifications [2]-[4] a phase-space statistical approach. The both models have limited ranges of applicability which can be formulated roughly as above 100 MeV for the cascade model and below 100 MeV for the exciton one. On the other hand, the exciton model was found to be a successful addition to the cascade description of nuclear reactions and was introduced into most of widely used cascade-based high energy transport codes [5]-[8] in the last years.

There are some problems in the frame of the cascade-exciton model which have not been decided up to the present. This is related first of all to the angular distributions of secondary nucleons which are in a systematical disagreement with experiment at very forward angles as well as at backward angles [8],[9]. These problems increase with the decrease of incident nucleon energy below 100 MeV. The usual explanation consists in neglecting quantum-mechanical effects such as the refraction at the nuclear surface, quantum diffraction, conservation laws for the angular momentum, parity etc. It should be noted, however, that the same problem persists even in the most complete quantum-mechanical Feshbach-Kerman-Koonin (FKK) preequilibrium theory [10].

The promising results in calculating the double-differential nucleon spectra from nucleon-induced reactions have been achieved recently in the frame of a new model primarily developed for simulation of nucleus-nucleus collisions – the quantum molecular dynamics (QMD) [10],[11]. In contrast to the cascade model, the QMD describes simultaneous motion of an incident particle and intranuclear nucleons. The time evolution of particles in the coordinate and momentum space is described by Newtonian equations and the stochastic two-body collision term in the form of Boltzmann-Uehling-Uhlenbeck (BUU). It has been found from the QMD calculations that two effects are important for the agreement with experiment at small and large angles: particle refraction at the nuclear surface and the use of realistic momentum distribution of nucleons inside nuclei including a high-momentum tail.

The high energy transport code HADRON [12] based on the cascade-exciton model was developed and successfully used for deciding different dosimetric problems [13]-[15]. Its essential distinction from other codes is more accurate physics of nucleon-induced reactions below 100 MeV where the program was carefully tested. In this paper we describe a new version of the

HADRON code – HADR99 – in part of the hadron event generator. Modifications, introduced into the cascade and exciton models in the last years, provide an essential improvement in prediction of the double differential cross sections from (N,xN')-reactions in a wide energy range. Some changes in the HADRON code were made 3-4 years ago but have not yet been published. The latest modifications are the following:

– new model of the nuclear potential well,
– simulation of particle refraction by the mean-field potential,
– new parametrization for the inverse reaction cross-sections,
– more accurate level densities for preequilibrium emission.

2. Model

The cascade model of nuclear reactions is based on the Fermi-gas model of nuclear matter in which a nucleus is represented as a gas of free nucleons in a nuclear potential well [16]. Collisions between nucleons are forbidden due to the Pauli principle. Nuclear potential in the Fermi-gas model is uniquely defined by the corresponding density of nuclear matter. This is a usual approach that was used earlier in the HADRON code as well. The refraction of particles at the nuclear surface is not generally considered in cascade codes. A possible reason is that such effects as refraction and reflection were found to be unsuccessful at the early stage of cascade model development [17]. The recent studies [10] and our calculations show that the refraction plays an important role in the cascade process.

A number of test calculations with different refraction models and nuclear potentials were performed to understand the main features of double differential cross-sections depending on the model parameters. It was found that the Fermi-gas nuclear potential should be replaced by deeper and wider potential well. As a result, we have taken a real part of an optical potential derived from the experiments on elastic and inelastic scattering of nucleons by nuclei. This potential is consistent with the nucleon density distribution: it is 1 fm wider assuming the effective radius of nuclear forces. Our model is described by the following equations.

The nucleon densities are defined by the Woods-Saxon distribution as earlier:

$$\rho_N(r) = \frac{\rho_{N0}}{1 + exp((r - R)/a)}, \tag{1}$$

where $R = 1.07 \cdot A^{1/3}\ fm$ and $a = 0.54\ fm$. The densities at the center of nucleus ρ_{N0} are calculated by normalizing distribution (1) to the total number of corresponding nucleons in a nucleus. The nuclear potential is described as

$$V_N(r) = \frac{V_{N0}}{1 + exp((r - R_V)/a_V)} + V_C(r), \tag{2}$$

with $R_V = (R + 1)\ fm$ and $a_V = 0.65\ fm$. V_{N0} is equal to

$$V_{N0} = -(52 \pm 33\frac{N - Z}{A})MeV, \tag{3}$$

where the symmetry term is positive for protons and negative for neutrons. The Coulomb potential $V_C(r)$ for neutrons is zero, for protons it is defined as

$$V_C(r) = \begin{cases} (Ze^2/2R_C)[3 - (r/R_C)^2] & , r < R_C \\ Ze^2/r & , r > R_C \end{cases} \tag{4}$$

The Coulomb radius was taken as $R_C = R_V$.

The radial dependences of neutron and proton potentials calculated by equations (2-4) for the ^{56}Fe nucleus are compared in Fig. 1 with the corresponding Fermi-gas potentials. The new model provides a wider and 8-10 MeV deeper potential well. As a result, the difference between two potentials at the nuclear surface amounts up to a factor of 2 and more. One of the consequences of these changes is that the role of nuclear periphery in a cascade process becomes much more essential, especially at low energies of incident nucleons.

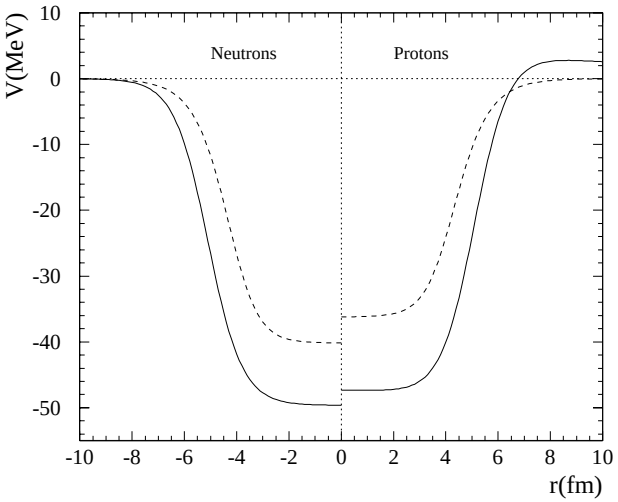

Fig. 1. Nucleon potentials for the ^{56}Fe nucleus. Solid curves – present model (2-4), dashed curves – Fermi-gas model.

For Monte Carlo simulation, a nucleus is divided into 8 radial zones with the average densities ρ_{Ni} and positive potentials V_{Ni} since we calculate all the kinetic energies from the bottom of potential well, as usual. The potentials V_{Ni} are used as Fermi energies that is maximum kinetic energies of nucleons in zone i. Nucleon momentum $\vec{P}_{Ni}$ is randomly distributed in such a prescription in the sphere of radius $P^F_{Ni} = \sqrt{2m_N V_{Ni}}$. The total potential for the cascade nucleons is defined as a sum of V_{Ni} and binding energy B_N: $U_{Ni} = V_{Ni} + B_N$. The constant value of the pion potential $U_{\pi i} = 25$ MeV remained in the program.

The kinetic energy T_0 of an incident hadron changes inside nucleus as $T = T_0 + U_i$. Particle trajectories are represented by a sequence of straight segments with different directions depending on a zone. The change of direction between zones (refraction) is a consequence of the jump in kinetic energy. It is described using the condition of continuous tangential component of particle momentum:

$$P' \sin\theta' = P \sin\theta, \tag{5}$$

where (P, P') are the scalar momenta in two zones and (θ, θ') are the corresponding angles between the particle direction and radius-vector from the center of nucleus to the point of particle transition to another zone. There are some cases in which equation (5) is violated: $\sin\theta' = P\sin\theta/P' > 1$. They correspond to internal reflection of particles by nuclear potential what is impossible for the smooth attractive potential well. We suppose therefore in such cases that $\sin\theta' = 1$. This condition is close to real situation that was checked by the test calculations using a smooth potential well without dividing it into discrete zones. The Coulomb potential outside a nucleus is assumed to be zero since the Coulomb deflection of charged hadrons is compensated by the refraction at the nuclear border due to the Coulomb barrier.

After the cascade stage, a residual nucleus is characterized by the excitation energy E^*, momentum $\vec{P}$ and initial particle-hole configuration $(p = p_\nu + p_\pi, h)$ where p_ν and p_π are the numbers of excited neutrons and protons. The process of nucleus deexcitation is considered further in the frame of preequilibrium exciton model including an equilibrium approach as a final stage. We follow basically the prescription of the exciton model [5] as described in our paper [12]. Its important advantage is the absence of free adjustable parameters. This is related first of all to the intranuclear transitions with changing the number of excitons whose probabilities were obtained in [5] using free nucleon-nucleon cross sections. The new charge state of excited nucleons (p_ν, p_π) after this process is calculated in HADR99 randomly using the

condition that $\sigma_{nn} = \sigma_{pp} \simeq \sigma_{np}/3$ below 100 MeV. The same approach is used after the surface absorption of cascade nucleons by an optical potential.

The main equation describing particle emission probalitities λ_j in the exciton model is the following:

$$\lambda_j(p,h,E^*,T) = \frac{2s_j+1}{\pi^2\hbar^3}\mu_j\sigma_j(T)T\frac{\omega(p-p_j,h,E^*-B_j-T)}{\omega(p,h,E^*)}R_j(p_\nu,p_\pi), \tag{6}$$

where s_j, μ_j and p_j are the spin, reduced mass and nucleon number for the j-th particle. $R_j(p_\nu,p_\pi)$ is a factor providing a charge conservation. Equation (6) contains only two functions of kinetic energy T of the emitted particle. They were modified in the HADR99 code compared to the previous version of HADRON. The exciton state densities are calculated taking into account the Pauli principle and finite depth of potential well [18]:

$$\omega(p,h,E^*) = \frac{g^n}{p!h!(n-1)!}\sum_{l=0}^{h}(-1)^l\frac{h!}{l!(h-l)!}(E^*-A_{ph}-l\bar{V}_N)^{n-1}\Theta(E^*-A_{ph}-l\bar{V}_N), \tag{7}$$

where $n = p+h$; g is the density of single-particle states; $A_{ph} = (p^2+h^2+p-3h)/4g$ is the Pauli principle correction; $\Theta(x)$ is the function which is unity if its argument is positive and zero otherwise; $\bar{V}_N$ is the average depth of nuclear potential well which was taken to be 38 MeV.

The usually used in the cascade-based codes Dostrovsky parametrization [19] of the inverse reaction cross sections is a rather rough approximation. We have made therefore a new parametrization which is formulated as follows:

$$\sigma_j(T) = [a_j + b_j max(0, 1-T/T_j)](1-V_j/T), \tag{8}$$

where V_j is the Coulomb potential; $T_j = 70p_j$ MeV; a_j and b_j are the smooth functions of nucleus atomic weight. Such a choice was dictated by a compromise between the accuracy of approximation and simplicity that enables one to perform the analytical integration of expression (6). The typical result of parametrization (8) for nucleons is shown in Fig. 2.

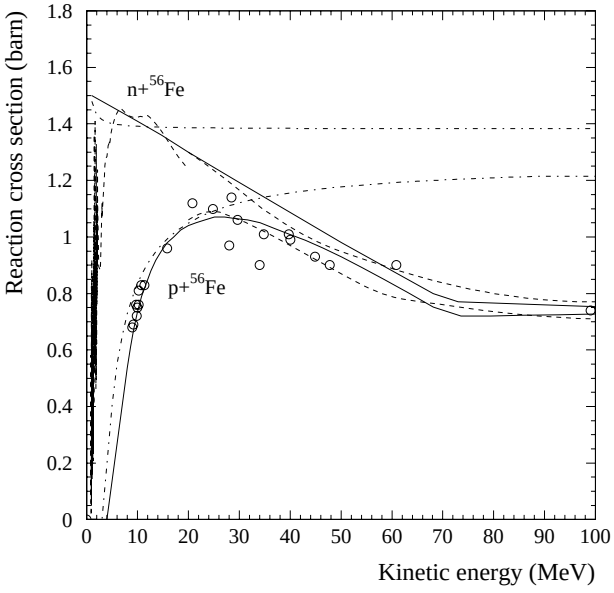

Fig. 2. Nucleon reaction cross sections for the ^{56}Fe nucleus. Dashed curve below 20 MeV – ENDF-B/VI [20], dashed curves above 20 MeV – parametrization [21]. Experimental points for protons are taken from [21], dashed-dot curves – Dostrovsky parametrization [19], solid curves – present parametrization (8).

In spite of large differences between the old and new state densities and cross sections, the changes in the angle-integrated nucleon spectra are relatively small at incident energies below 100 MeV where a large number of experiments are available. This is explained by the fact that the Dostrovsky parametrization describes enough accurately the ratio of cross sections for neutrons and protons which are the main emitted particles at a preequilibrium stage. At the same time, the new cross sections (8) strongly improve the preequilibrium spectra of complex particles ($d, t, ^3He, \alpha$). This enables one to exclude from equation (6) any phenomenological functions, often used to describe the formation of complex particles, which cannot be obtained from microscopic reversibility. The effect of finite depth of potential well in expression (7) becomes important at incident energies above 100-200 MeV where residual nuclei after cascade may have high excitation energies.

The angular distribution of preequilibrium ejectiles is simulated by the method slightly different from [5]. The nucleus momentum $\vec{P}$ is attributed to p excitons instead of $p+h$ as in [5]. We suppose that holes give rise to the excitation energy only. Collisions of excited particles with intranuclear nucleons are calculated from the isotropic distribution in the center of mass system. This distribution is naturally tranformed into anisotropic one after the transition to the system of moving nucleus and, further, to the laboratory system.

The density of single-particle states was taken as $g = A/13$. The particle emission probabilities at the equilibrium stage are calculated by equation (6) with changing $R_j(p_\nu, p_\pi) \to 1$ and $\omega(p, h, E^*) \to \omega_{eq}(E^*) \sim \exp(2\sqrt{aE^*})$ where the energy-dependent parametrization [22] is used for the level density parameter a. This parametrization effectively takes into account the shell and pairing effects in nuclei.

The other important distinctions of our cascade-exciton model from the usual approaches are the following:

1. At all stages of nuclear reaction, relativistic kinematics with exact energy and momentum conservation, taking into account recoil nucleus, is used.

2. Hadron-nucleus reaction cross sections are calculated using the parametrization [21] based on experimental data and optical model calculations. This is important at low projectile energies where the cascade model fails in predicting nonelastic cross sections.

3. The neutron and proton binding energies B_N are calculated from a database of experimental nuclear masses [23] at all stages, instead of usually used in cascade codes constant value of 7-8 MeV. In those cases when the database does not contain information for at least one nucleus (nucleus before or after particle emission is unstable), the Cameron semiempirical formula [24] is applied.

4. In addition to Z and A, we characterize target nucleus by the energy E_1^* of the first excited state. It may amount up to some MeV for light even-even nuclei (4.44 MeV for ^{12}C and 6.05 MeV for ^{16}O, for example). The quasielastic (p, p') and (n, n')-events with $E^* < E_1^*$ are forbidden in the HADRON code since they correspond to the elastic scattering channel. The Pauli principle subroutine was modified to take into account this effect at the cascade stage. The same veto is applied at the preequilibrium stage.

5. The decrease of nucleon density during the cascade stage ("treiling" effect), important for light nuclei above 1 GeV, is taken into account similar to the method [25]. The cascade process is calculated in a real time scale approximately in spite of the cascade particle trajectories are considered alternately. The characteristics of particles are written in a stack correspondingly to the time of their appearance. This stack is redefined after each collision so as the earliest particle is taken from the stack every time. The nucleon densities ρ_{Ni} are redefined as well after each

collision or absorption of cascade particles. This approach was tested by the nuclear emulsion experiments described in [16].

6. The transition from the cascade to preequilibrium stage is carried out using the imaginary part of an optical potential as described in [12]. The other conditions of cascade particle absorption are formulated as $T_n < U_{ni}$ for neutrons and $T_p < U_{pi} + V_p$ for protons, where V_p is the value of Coulomb barrier. The first mechanism plays the main role in the cascade cut-off so the change of minimum kinetic energies of cascade particles in the limits of some MeV does not influence the final results.

3. Results and discussion

For comparison of the HADR99 code with experiment, we have taken double differential cross sections of (N, xN') reactions measured with high enough resolution in wide ranges of secondary nucleon energies and angles. Our discussion starts from the projectile energy region below 100 MeV where all the calculational models have serious problems.

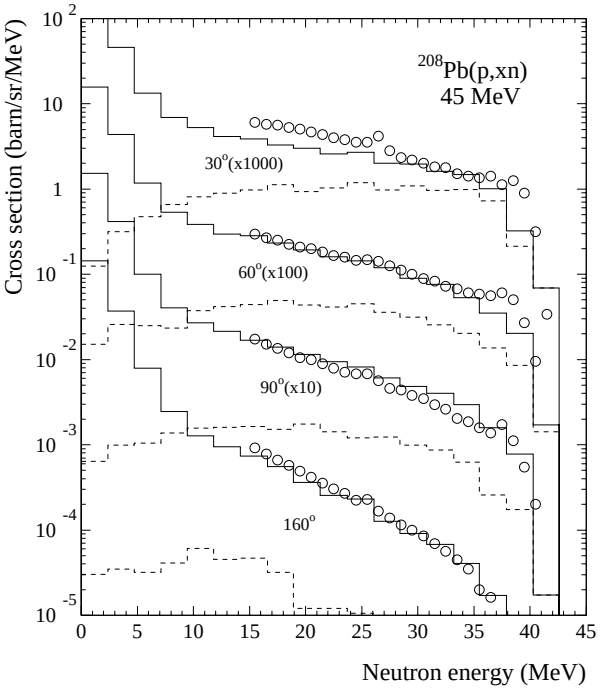

Fig. 3. Neutron energy spectra at different angles for the reaction p(45 MeV)+^{208}Pb. Points – experimental data [26], solid histograms – total calculated spectra, dashed histograms – cascade component.

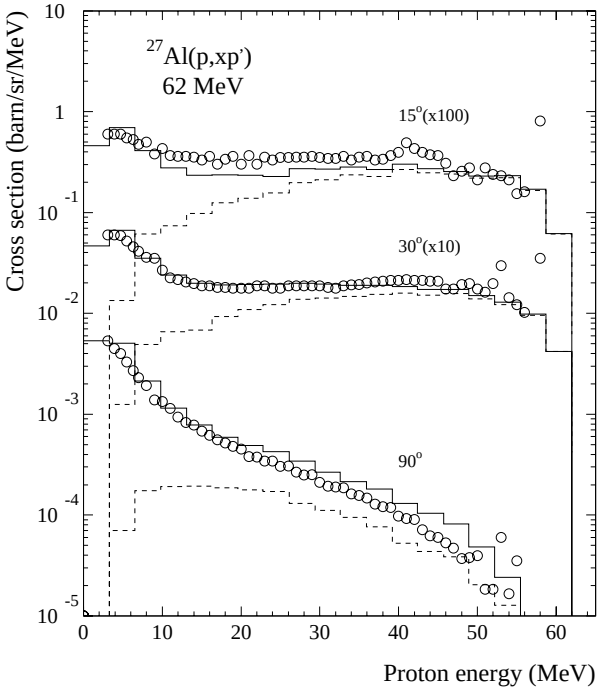

Fig. 4. Same as in Fig. 3 for the reaction p(62 MeV)+^{27}Al [27].

In Figs. 3 and 4, the HADR99 calculations are compared with the nucleon energy spectra at different angles measured for the reactions $^{208}\mathrm{Pb}(p, xn)$ at 45 MeV [26] and $^{27}\mathrm{Al}(p, xp')$ at 62 MeV [27]. The calculated cascade components of the total spectra are shown in the same figures. One can see that two different mechanisms play the main role in the considered cases. The proton spectra above 20 MeV from ^{27}Al are defined mainly by the cascade stage whereas most of the secondary neutrons above 10 MeV from ^{208}Pb are due to the preequilibrium process. This is explained by effective absorption of cascade particles with the large ^{208}Pb nucleus and

lower incident energy in this case. The agreement between theory and experiment in both cases is in the limits of 30%, as a rule, in the whole range of energies and angles.

The following four figures are very important for our comparison due to the rare possibility of simultaneous testing both the proton and neutron secondary spectra from proton-induced reactions. Figs. 5 and 6 show the data for ^{90}Zr at the incident energy of 80 MeV. The experimental and theoretical spectra from ^{27}Al at 90 MeV are presented in Figs. 7 and 8. The calculated results for the ^{90}Zr nucleus agree well with experiment for proton as well as for neutron spectra. This is not the case for ^{27}Al where the HADR99 data show systematical underprediction of the proton cross sections and overprediction for neutrons in the limits of 20-30%, on the average. These discrepancies are mainly attributed to the features of the cascade process in the light ^{27}Al nucleus that is qualitatively confirmed by Fig. 4. The sharp quasielastic peaks in the $^{27}\mathrm{Al}(p, xp')$ experimental spectra in Figs. 4 and 7 are explained by the collective excitation of low-lying levels which is not described by the cascade model.

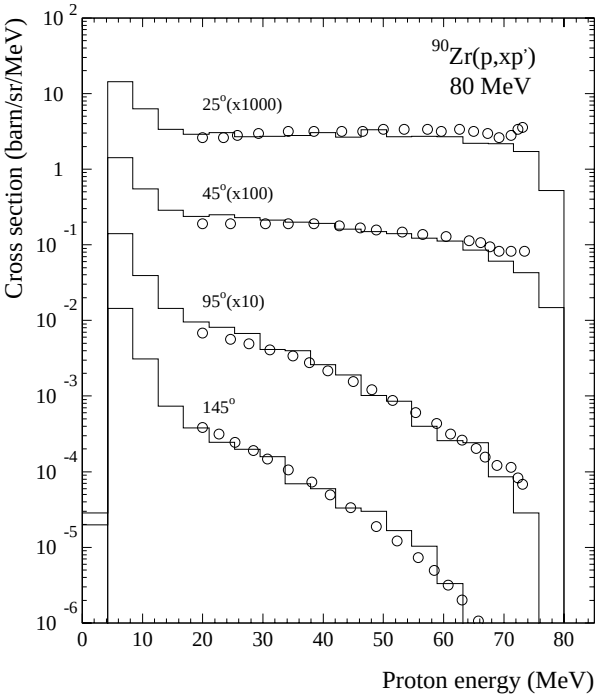

Fig. 5. Proton energy spectra at different angles for the reaction p(80 MeV)+^{90}Zr. Points – experimental data [28], histograms – calculated spectra.

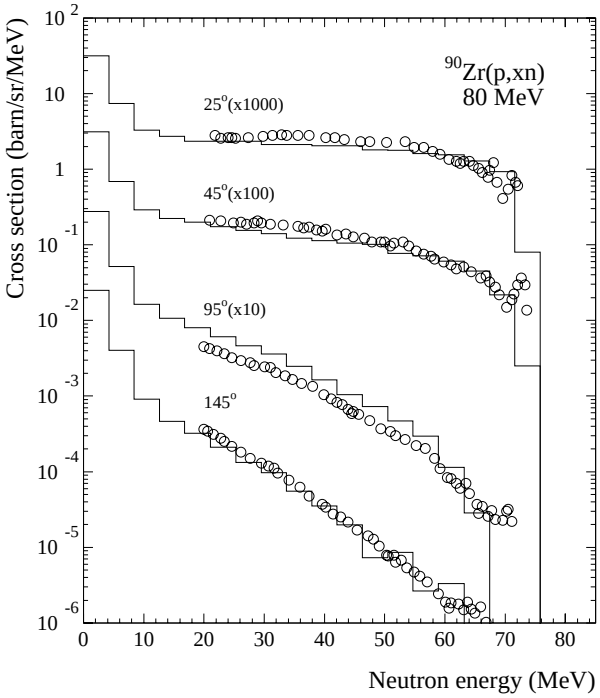

Fig. 6. Same as in Fig. 5 for secondary neutron spectra [29].

Figs. 7 and 8 also demonstrate the dependence of calculated nucleon spectra on the refraction process and nuclear potential model. The proton spectra, shown by the dashed histogram in Fig. 7, were calculated without refraction and with the Fermi potential well. The corresponding neutron spectra in Fig. 8 were obtained with the same potential but with refraction. It should be mentioned that neutron and proton results show in this case similar dependence on the cascade model parameters, therefore, the data for one type of nucleons are applicable qualitatively to another type. It can be seen from the presented data that the refraction effects play an important role at all angles for incident energies below 100 MeV, in contrast to the conclusion [10] made for the energy range above 100 MeV. The second conclusion on the importance of high-momentum

component in the nucleon momentum distribution for the description of the backward spectra drawn in [10] is not supported as well by the data from Fig. 8 where the softer potential leads to increased neutron emission at 90^o and 120^o.

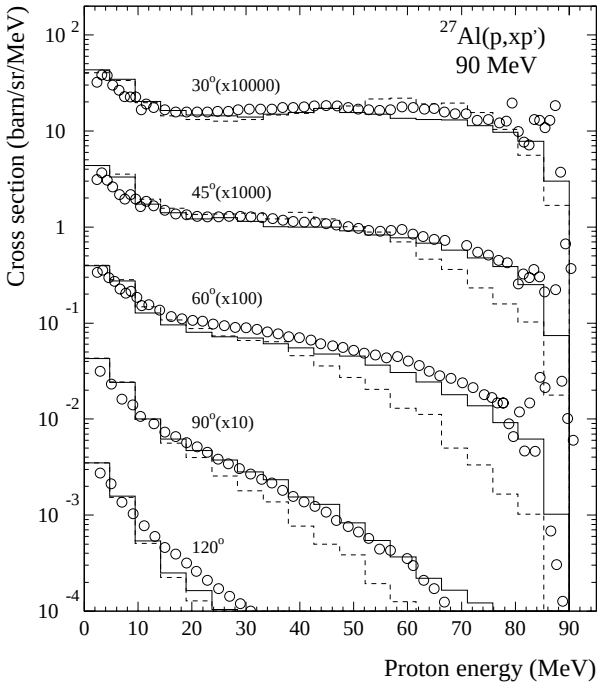

Fig. 7. Proton energy spectra at different angles for the reaction p(90 MeV)+^{27}Al [30]. Solid histograms – HADR99 calculation. Dashed histograms – calculation with the Fermi-gas potential and without refraction.

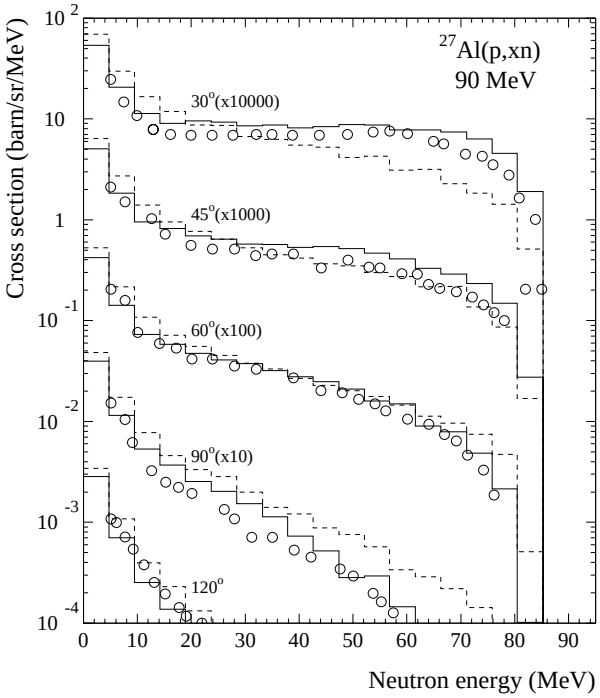

Fig. 8. Neutron energy spectra at different angles for the reaction p(90 MeV)+^{27}Al [31]. Solid histograms – HADR99 calculation. Dashed histograms – calculation with the Fermi-gas potential.

In fact, there is a complex interference picture of different effects dependent on the nuclear potential model such as refraction, energy dependence of nucleon-nucleon cross sections, Pauli principle blocking, surface absorption, etc. The relative importance of these effects also depends on target nucleus and projectile energy so any definite conclusions on one of the model parameters cannot be easily drawn from the comparison of calculated and experimental data. Nevertheless, the potential widthness was found to be one of the most important model parameters in our test calculations.

In Figs. 9-12, we present the comparison with the LANL experiments [32],[33] for (p, xn)-reaction from 113 to 800 MeV made in a wide energy range of secondary neutrons. These data confirm the suggestion that 100 MeV is a critical energy for the cascade model. Above this energy, it becomes much less sensitive to the details of potential well and refraction. Fig. 9 shows that the calculations with the old potential and without refraction give nearly the same spectra as HADR99 except the very forward angle of 7.5^o. The refraction process washes off the quasifree scattering peak observed in the cascade calculations but this effect disappears at higher energies (Fig. 10). In Fig. 10, the comparison of the old and new preequilibrium models is also shown. The noticeable difference between two calculations at energies of some tens of MeV is explained mainly by using the improved exciton state densities (7) in HADR99 which cut off the low energy part of emission spectra at high excitation energies.

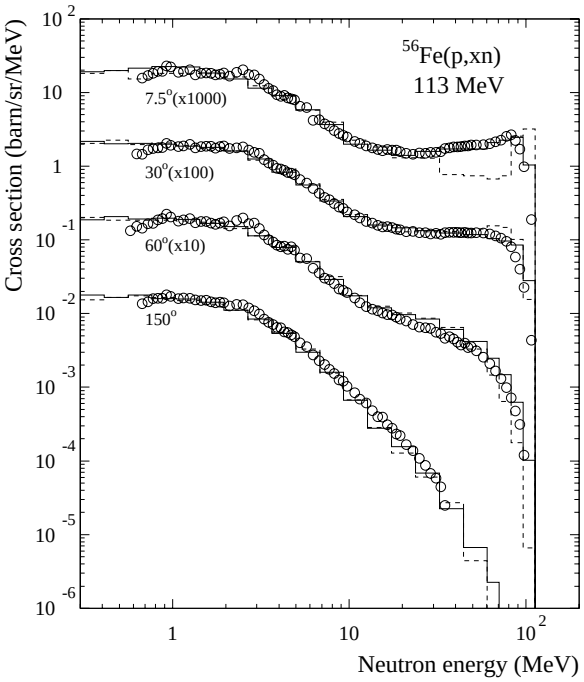

Fig. 9. Neutron energy spectra at different angles for the reaction p(113 MeV)+^{56}Fe [32]. Solid histograms – HADR99 calculation. Dashed histograms – calculation with the Fermi-gas potential and without refraction.

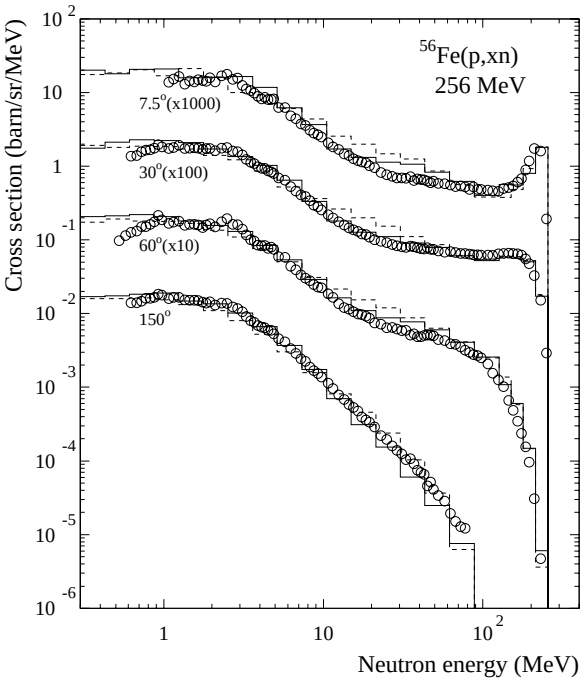

Fig. 10. Neutron energy spectra at different angles for the reaction p(256 MeV)+^{56}Fe [32]. Solid histograms – HADR99 calculation. Dashed histograms – calculation with the old preequilibrium model.

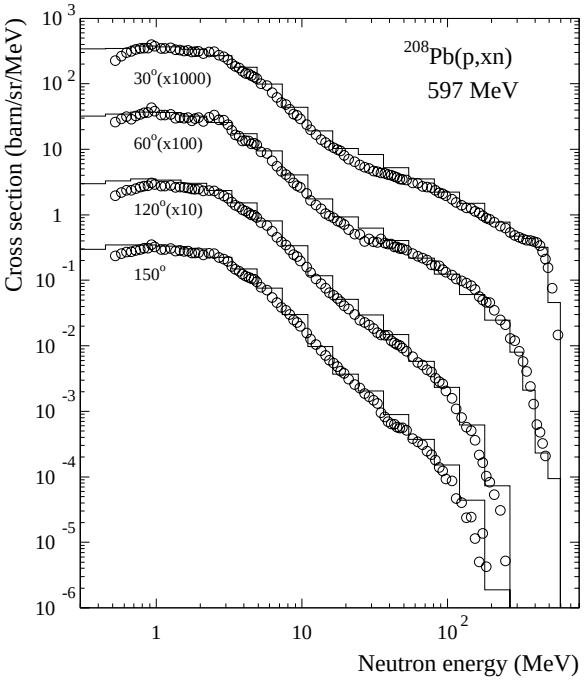

Fig. 11. Neutron energy spectra at different angles for the reaction p(597 MeV)+^{208}Pb [33].

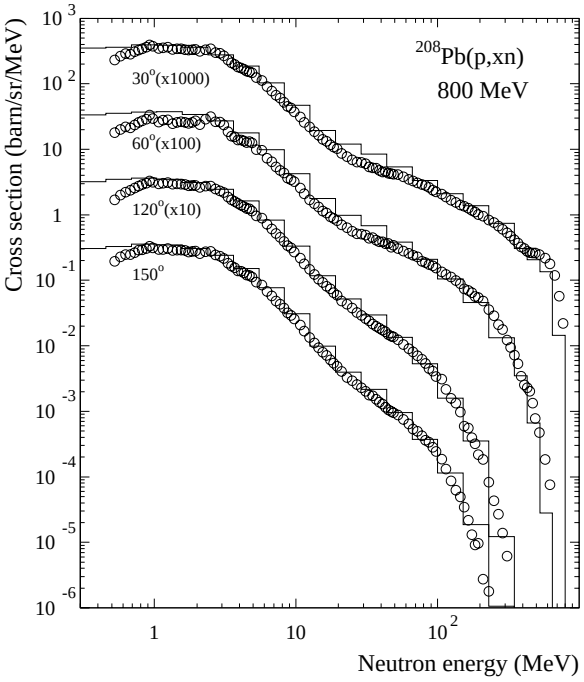

Fig. 12. Same as in Fig. 11 for 800 MeV incident protons [33].

The systematical discrepancy between the calculated and experimental data below 1 MeV can be seen from Figs. 10-12. This is explained by the simplified neutron-nucleus reaction cross sections used in our calculations. The energy dependence $\sigma_n(T)$ is rather complicated in a low energy region, in contrast to equation (8), and is strongly influenced by the shell and pairing effects in atomic nuclei similar to the behavior of nuclear level densities at low excitation energies. For most intermediate and heavy nuclei, there is a threshold picture of neutron-nucleus cross section which leads to the decrease of low energy neutron emission observed in the considered cases. The improved description of reaction cross sections will be a subject of future work.

The further progress is also connected with taking into account some microscopic and quantum effects. These are the conservation laws for angular momentum, parity and isospin, discrete excitation levels, shell and pairing effects, collective nuclear excitations etc. Not all of them are of equal importance. For light nuclei, for example, the discrete structure of excitation levels is an essential factor at all incident energies. The other effects may be important for some reaction channels below some tens of MeV.

The study of nuclear potential model should be prolonged as well. This is related, for instance, to the energy dependence of nuclear potential which was found in the optical model of nuclear reactions. Very different approach to constraining nuclear potential is used in the QMD model [11]. In this case, the Skyrme parametrization [34] is applied to describe a nuclear potential as a superposition of attractive and repulsive terms depending on the density of nuclear matter. The repulsive short-range term is important for nucleus-nucleus reactions where a strong compression of nuclear matter at the early stage of reaction and large fluctuations of nucleon density take place. This is not the case for nucleon-induced reactions where the attractive potential seems to be sufficient. Another distinction of QMD from the cascade model – the description of simultaneous motion of intranuclear nucleons during the reaction development – is important only at the relatively slow preequilibrium stage which is successfully described in HADR99 by the statistical exciton model. The random sampling of Fermi nucleon momentum and time-independent nuclear potential are good enough approximations for the fast cascade stage.

One more important point of QMD to be discussed is the two-body collision term. Comparison of the QMD calculations [11] with experimental data from 113 to 800 MeV shows that the theory strongly underestimates high energy tails of neutron spectra corresponding to hard nucleon-nucleon collisions. Moreover, the calculated results demonstrate the obvious violation of the energy conservation law in these collisions: neutron spectra extend up to 150 and 300 MeV for 113 and 256 MeV incident protons, correspondingly. Our interest to QMD was provoked by new physics applied in this theory which promises new ideas for the cascade-exciton model. Unfortunately, we should conclude that the QMD model [11] is not elaborated enough to draw any certain conclusion from the comparison with experiment.

The cascade-exciton model described in this paper agrees well with experiment and has no intrinsic limitations as was discussed above. The most serious problem observed in our tests is the systematical deviation from the experimental neutron and proton spectra for the $^{27}\mathrm{Al}(p, xN)$-reactions at 90 MeV (Figs. 7 and 8). A possible explanation consists in changing the free nucleon-nucleon cross sections in a nuclear matter. The most important factor of this change – the Pauli principle – is taken into account in our model. An additional mechanism may be found, in our opinion, in the "pickup" formation of fast deuterons in nuclei what is impossible in free (n, p)-collisions. This effect does not influence the (p, p) and (n, n) cross sections but reduces the neutron-proton elastic scattering cross section. The first promising results in the quantitative analysis of this process were obtained during the preparation of the present paper.

4. Conclusions

In spite of some deviations from experiment, the improved cascade-exciton model realized in the HADR99 code describes the (N, xN') double differential cross sections with an average accuracy better than 30% in wide ranges of incident energies and target nuclei. We would remind that our model does not contain any adjustable input parameters for separate nuclei. This is an evidence of high quality of the physical model essentially based on experimental data. The cascade-exciton model is open for future improvements, some of them have been discussed above. As compared to the QMD approach, the model has considerable advantages in the nucleon- and pion-induced reactions since it is much more simple and fast. For nucleus-nucleus reactions, density fluctuations of nuclear matter are of great importance and should be taken into account.

References

[1] N.Metropolis et al. Phys. Rev. **110**, 185 (1958); **110**, 204 (1958).

[2] J.J.Griffin. Phys. Rev. Lett. **17**, 478 (1966).

[3] G.Mantzouranis, H.A.Weidenmüller and D.Agassi. Phys. Lett. **57B**, 220 (1975).

[4] M.Blann, W.Scobel and E.Plechaty. Phys. Rev. **C30**, 1493 (1984).

[5] K.K.Gudima, S.G.Mashnik and V.D.Toneev. Nucl. Phys. **A401**, 329 (1983).

[6] R.E.Prael and H.Lichtenstein. *User Guide to LCS: The LAHET Code System*. LANL Report LA-UR-89-3014, Los Alamos, 1989.

[7] A.Fasso, A.Ferrari, J.Ranft et al. *FLUKA92*. Workshop on Simulating Accelerator Radiation Environments. Santa Fe, USA, 1993.

[8] K.Ishibashi, N.Yoshizava, H.Takada and Y. Nakamura. *High Energy Transport Code HETC-3STEP Applicable to Incident Energies below 100 MeV*. Proc. of Int. Conf. on Nucl. Data for Sci. and Technol. Gatlinburg, Tennessee, 1994.

[9] R.E.Prael. Report LANL LA-87545-NM, Los Alamos, 1989.

[10] S.Chiba, M.B.Chadwick, K.Niita et al. Phys. Rev. **C53**, 1824 (1996).

[11] K.Niita, S.Chiba, T.Maruyama et al. Phys. Rev. **C52**, 2620 (1995).

[12] E.N.Savitskaya and A.V.Sannikov. Radiat. Prot. Dosim. **60**, 135 (1995).

[13] A.V.Sannikov and E.N.Savitskaya. Radiat. Prot. Dosim. **70**, 383 (1997).

[14] A.V.Sannikov, V.Mares and H.Schraube. Radiat. Prot. Dosim. **70**, 291 (1997).

[15] I.L.Azhgirey, I.A.Kurochkin, A.V.Sannikov and E.N.Savitskaya. Nucl. Instrum. Meth. Phys. Res. **A408**, 535 (1998).

[16] V.S.Barashenkov and V.D.Toneev. *Interaction of High Energy Particles and Nuclei with Nuclei*. Moscow: Atomizdat (1972).

[17] K.Chen, Z.Fraenkel, G.Friedlander et al. Phys. Rev. **166**, 949 (1968).

[18] F.A.Zhivopistsev, E.J.Käbin and V.G.Sukharevsky. *Preequilibrium Models of Nuclear Reactions*. Moscow State University (1987).

[19] I.Dostrovsky, Z.Fraenkel and G.Friedlander. Phys. Rev. **116**, 683 (1959).

[20] ENDF-B/VI in IAEA-NDS-100, Rev. 4, June 1992, Vienna.

[21] V.S.Barashenkov. *Cross Sections of Hadron Interactions with Nuclei*. Dubna: JINR (1993).

[22] E.A.Cherepanov and A.S.Iljinov. Nucleonika. **25**, 611 (1980).

[23] A.Wapstra and N.Gove. Nuclear Data Tables **A9**, 265 (1971).

[24] A.G.W.Cameron. Canad. J. Phys. **35**, 1021 (1957).

[25] V.S.Barashenkov, A.S.Iljinov and V.D.Toneev. Preprint JINR P2-5280, Dubna (1970).

[26] R.R.Doering, D.M.Patterson and A.Galonsky. Phys. Rev. **C12**, 378 (1975).

[27] F.E.Bertrand and R.W.Peelle. Phys. Rev. **C8**, 1045 (1973).

[28] A.A.Cowley, A. van Kent, J.J. Lawrie et al. Phys. Rev. **C43**, 678 (1991).

[29] M.Trabandt, W.Scobel, M.Blann et al. Phys. Rev. **C39**, 452 (1989).

[30] J.R.Wu, C.C.Chang and H.D.Holmgren. Phys. Rev. **C19**, 698 (1979).

[31] A.M.Kalend, B.D.Anderson, A.R.Baldwin et al. Phys. Rev. **C28**, 105 (1990).

[32] M.M.Meier, C.A.Goulding, G.L.Morgan and J.Ullmann. Nucl. Sci. Eng. **104**, 339 (1990).

[33] W.B.Amian, B.C.Byrd, C.A.Goulding et al. Nucl. Sci. Eng. **112**, 827 (1992).

[34] T.H.R.Skyrme. Nucl. Phys. **9**, 615 (1959).

Received July 7, 1999

А.В.Санников, Е.Н.Савицкая
Физика программы HADRON: современное состояние и сравнение с экспериментом.

Оригинал-макет подготовлен с помощью системы LaTeX.
Редактор Е.Н.Горина. Технический редактор Н.В.Орлова.

Подписано к печати 08.07.99. Формат 60 × 84/8. Офсетная печать.
Печ.л. 1.5. Уч.-изд.л. 1.2. Тираж 160. Заказ 166. Индекс 3649.
ЛР №020498 17.04.97.

ГНЦ РФ Институт физики высоких энергий
142284, Протвино Московской обл.

Индекс 3649

П Р Е П Р И Н Т 99-37, И Ф В Э, 1999